Nusselt number scaling in tokamak plasma turbulence

Cite as: Phys. Plasmas **12**, 052309 (2005); https://doi.org/10.1063/1.1895165
Submitted: 21 January 2005 . Accepted: 01 March 2005 . Published Online: 28 April 2005

K. Takeda, S. Benkadda, S. Hamaguchi, and M. Wakatani

Nusselt number scaling in tokamak plasma turbulence

K. Takeda[a] and S. Benkadda[b]
Department of Fundamental Energy Science, Kyoto University, Gokasho, Uji, Kyoto 611-0011, Japan and Equipe Dynamique des Systèmes Complexes, UMR 6633, CNRS-Université de Provence, Marseille, France

S. Hamaguchi[c]
STAMIC, Graduate School of Engineering, Osaka University, 2-1 Yamadaoka, Suita, Osaka 565-0871, Japan

M. Wakatani[d]
Department of Fundamental Energy Science, Kyoto University, Gokasho, Uji, Kyoto 611-0011, Japan

(Received 21 January 2005; accepted 1 March 2005; published online 28 April 2005)

Anomalous heat transport caused by ion temperature gradient (ITG) driven turbulence in tokamak plasmas is evaluated from numerical simulations of the two-dimensional (2D) partial-differential equations of the ITG model and of a reduced 1D version derived from a quasilinear approximation. In the strongly turbulent state, intermittent bursts of thermal transport are observed in both cases. In the strongly turbulent regime, the reduced model as well as the direct numerical simulation show that the Nusselt number Nu (normalized heat flux) scales with the normalized ion pressure gradient K_i as $\mathrm{Nu} \propto K_i^{1/3}$. Since the Rayleigh number for ITG turbulence is proportional to K_i, the Nusselt number scaling for ITG turbulence is thus similar to the classical thermal transport scaling for Rayleigh–Bénard convections in neutral fluids. © *2005 American Institute of Physics*.
[DOI: 10.1063/1.1895165]

I. INTRODUCTION

Turbulence driven by microinstabilities in magnetically confined fusion experimental devices such as tokamaks and stellarators has been extensively studied in an attempt to control and suppress anomalously large heat and particle transport observed in those devices. Understanding the nature of such microturbulence is generally considered to be one of the most important issues for confinement studies of fusion reactors.

The ion temperature gradient (ITG) mode (also known as the η_i mode) is an electrostatic microinstability with low frequencies. It is a modified ion acoustic wave coupled with the drift wave, which becomes unstable due to the free energy carried by an ion acoustic wave along the magnetic field lines when the ratio of the ion temperature gradient to density gradient becomes sufficiently large.[1] The ITG driven turbulence is generally regarded as the main cause of anomalous ion thermal transport in the hot core regions of tokamaks and stellarators.

The ITG mode has two branches, i.e., slab[2–5] and toroidal modes.[6–10] The toroidal ITG mode is driven by the Rayleigh–Taylor interchange mechanism and has essentially two-dimensional fluid instability characteristics.[6,9] The toroidal ITG mode is localized in the outer region of the torus and generally has a higher growth rate than the slab mode in toroidal magnetic geometry. In the present work, therefore, we focus on the toroidal ITG mode.

In the previous works,[11,10] the authors presented a low degree-of-freedom (i.e., low dimensional) model with the first 18 lowest order components for the toroidal ITG mode, which consists of the 18 ordinary differential equations (ODEs). In numerical simulations based on this model, intermittent bursts of thermal transport are observed when the system becomes sufficiently unstable. The intermittency is caused by the competition among three mechanisms, i.e., (1) the onset of ITG instability, (2) the generation of sheared flows, and (3) viscous damping of the sheared flows, as summarized in Ref. 10. To the best of the authors' knowledge, the 18 ODE model is the lowest order model derived from the full ITG fluid model that exhibits intermittent transport, similar to what is observed in more complete models.[12,13] For example, Lin *et al.*[14] have shown intermittent oscillations of ion thermal transport in large-scale gyrokinetic simulations for ITG driven turbulence. In another work using also gyrokinetic simulations, a period-doubling route to chaos with nonlinear oscillations has been observed close to the marginal stability during the nonlinear evolution of the modulation instability with monochromatic pump wave.[15] Using a spectral predator-pray model which couples drift waves with zonal flow excitations, a bursty behavior was also found near marginal stability.[16,17]

The solutions obtained from the 18 ODEs, however, usually differ from those of the original partial differential equations (PDEs) governing the toroidal ITG mode. In this paper, we first solve the original PDEs numerically and compare the thermal transport scaling obtained from these equations with that from the 18 ODE models It is shown that there is a significant quantitative difference in thermal transport scaling between these two models. We also solve numerically a

[a]Electronic mail: takeda@up.univ-mrs.fr
[b]Electronic mail: benkadda@up.univ-mrs.fr
[c]Electronic mail: hamaguch@ppl.eng.osaka-u.ac.jp
[d]Deceased.

one-dimensional (1D) model for the ITG mode, which is a quasilinear version of the PDE model mentioned above but has more mode structures in the radial direction (i.e., the direction of the ion temperature gradient) than those of the 18 ODE model. The 1D simulation results are compared with those obtained from the full PDE and 18 ODE models. Let us note that similar 1D models were derived for resistive interchange turbulence as well as for resistive ballooning turbulence in previous works,[12,18] where it was also shown that intermittent bursts (so-called avalanches) occur when the system is in the strongly turbulent state.

In this work, based on both 1D and full PDE models of ITG turbulence, we shall present the anomalous thermal transport scalings in the hot core region of a tokamak plasma as the Nusselt number dependence on the normalized ion pressure gradient. In the edge region of a tokamak plasma, on the other hand, other types of instabilities such as resistive interchange modes play more significant roles in determining the thermal transport.[19]

The rest of this paper is organized as follows. In Sec. II, the PDEs governing the toroidal ITG mode are presented. The linear analysis of these equations as well as the numerical algorithm to solve them are also discussed briefly there. In Secs. III and IV, simulation results are shown for both full PDE and 1D models. Discussion and conclusions are given in Sec. V.

II. MODELS

A. Toroidal ITG equations

The following vorticity and ion pressure equations are known to describe the toroidal ITG mode:[6]

$$\frac{\partial}{\partial t}(\nabla_\perp^2\phi-\phi)+[\phi,\nabla_\perp^2\phi]=(1-g+K_i\nabla_\perp^2)\frac{\partial\phi}{\partial y}-g\frac{\partial p}{\partial y}+\mu\nabla_\perp^2\nabla_\perp^2\phi \tag{1}$$

and

$$\frac{\partial p}{\partial t}+[\phi,p]=-K_i\frac{\partial\phi}{\partial y}+\kappa\nabla_\perp^2 p, \tag{2}$$

where

$$[a,b]=\frac{\partial a}{\partial x}\frac{\partial b}{\partial y}-\frac{\partial a}{\partial y}\frac{\partial b}{\partial x}$$

are Poisson brackets. Here ϕ is the electrostatic potential, p is the ion pressure, g is the effective gravity due to the magnetic curvature, K_i is the ion pressure gradient, μ is the viscosity, and κ is the thermal conductivity. The position in the slab is given by (x,y) with the x and y directions corresponding to the radial and poloidal directions in a toroidal geometry and t represents time. Note that the gradients of mean quantities (such as mean ion temperature and density gradients) are present in the x direction only. The quantities used in the equations above follow the standard normalizations.[6] The normalized ion pressure gradient K_i is defined as $K_i=(1+\eta_i)T_i/T_e$ with $\eta_i\equiv L_n/L_{Ti}=d\ln T_i/d\ln n_0$, where T_i, T_e, and n_0 denote the equilibrium ion and electron temperatures and plasma density, respectively, and L_n and L_{Ti} denote the scale lengths for the equilibrium density and ion temperature gradients.

The toroidal ITG mode is driven by the Rayleigh–Taylor interchange mechanism. This mechanism is essentially the same as those of the Rayleigh–Bénard convection in neutral fluids and the resistive interchange instability in the edge plasmas. Based on this fact, we can define the following Rayleigh number Ra for ITG mode similar to those of the above two instabilities as

$$\mathrm{Ra}\equiv gK_iL_x^3/(\mu\kappa),$$

where L_x is the domain size in the x direction. The Rayleigh number is the ratio of the buoyancy force to viscous force, and characterizes the effect of driving force which generates thermal convections in the system. We note that the Rayleigh number is proportional to the ion pressure gradient, i.e., $\mathrm{Ra}\propto K_i$.

B. Linear analysis

Let us now discuss the linear growth rates of toroidal ITG modes given by the equations above. Assuming fluctuations depend on the position (x,y) and time t in the form $\exp(\mathrm{i}k_xx+\mathrm{i}k_yy-\mathrm{i}\omega t)$, we linearize Eqs. (1) and (2) and obtain the dispersion relation as follows:

$$[-\mathrm{i}(1+k_\perp^2)\omega+\mathrm{i}k_y(1-g-K_ik_\perp^2)+\mu k_\perp^4](-\mathrm{i}\omega+\kappa k_\perp^2)-gK_ik_y^2=0.$$

By solving this quadratic equation for the complex wave frequency ω, we obtain

$$\omega=\frac{1}{2(1+k_\perp^2)}\{k_y(1-g-K_ik_\perp^2)-\mathrm{i}[\kappa k_\perp^2(1+k_\perp^2)+\mu k_\perp^4]\pm\sqrt{D_k}\}$$

with

$$D_k=\{k_y(1-g-K_ik_\perp^2)+\mathrm{i}[\kappa k_\perp^2(1+k_\perp^2)-\mu k_\perp^4]\}^2-4(1+k_\perp^2)gK_ik_y^2.$$

From the linear growth rate $\gamma=\mathrm{Im}(\omega)$ estimated from the above expression, one readily finds that the growth rate becomes the largest when the wave numbers k_x and k_y satisfy

$$k_x^2\ll k_y^2\sim k_\perp^2=\frac{1-g}{K_i}.$$

In what follows, we select the mode satisfying

$$k_x=k_y/2=[(1-g)/5K_i]^{1/2} \tag{3}$$

as the fundamental mode and solve the nonlinear dynamics of it and its harmonics numerically.

C. Numerical procedures

Equations (1) and (2) are solved in the domain $0\leqslant x\leqslant L_x$ and $0\leqslant y\leqslant L_y$, where we set $L_x=\pi/k_x$ and $L_y=2\pi/k_y$ for k_x and k_y given by Eq. (3). We use the spectrum method in the x and y directions and expand ϕ and p into the Fourier series as follows:

$$\phi(t,x,y) = \sum_{\ell=1}^{N_x} \sum_{m=0}^{N_y} [\hat{\phi}^c_{\ell,m}(t)\sin(\ell k_x x)\cos(m k_y y) + \hat{\phi}^s_{\ell,m}(t)\sin(\ell k_x x)\sin(m k_y y)], \quad (4)$$

$$p(t,x,y) = \sum_{\ell=1}^{N_x} \sum_{m=0}^{N_y} [\hat{p}^c_{\ell,m}(t)\sin(\ell k_x x)\cos(m k_y y) + \hat{p}^s_{\ell,m}(t)\sin(\ell k_x x)\sin(m k_y y)], \quad (5)$$

where ℓ and m are the mode numbers and k_x and k_y are the minimum wave numbers in the x and y directions. Note that we have N_x and N_y+1 modes in the the x and y directions. By substituting Eqs. (4) and (5) into Eqs. (1) and (2), we obtain ODEs for the Fourier coefficients $\hat{\phi}^{c,s}_{\ell,m}$ and $\hat{p}^{c,s}_{\ell,m}$. Note that the 18 ODE model presented in Ref. 10 is reproduced if one sets $N_x=3$ and $N_y=1$.

Each Fourier component is numerically solved in time with the fifth-order Runge–Kutta method. From the solutions, we evaluate the total kinetic energy of the system defined as

$$K^{\text{total}} = \frac{1}{2}\int [\phi^2 + (\nabla_\perp \phi)^2] dV/V = \frac{1}{2}\langle \phi^2 + (\nabla_\perp \phi)^2 \rangle_V$$

as a function of time, where $\int dV/V = \langle\ \rangle_V$ denotes the volume average. The mean poloidal flow is the $m=0$ component of flow in the y direction, i.e., $V_y = \int(-\partial\phi/\partial x)dy/L_y = -\langle \partial\phi/\partial x\rangle_y$, and its kinetic energy is given by

$$K_0 = \sum_{\ell=1}^{N_x} \frac{1}{4}(1+\ell^2 k_x^2)(\phi^c_{\ell,0})^2.$$

Similarly the kinetic energy of the (ℓ,m) component of fluctuations $(m\neq 0)$ may be evaluated through the relations $v_x = \partial\phi/\partial y$ and $v_y = -\partial\phi/\partial x$ as

$$K_{\ell,m} = \frac{1}{8}(1+\ell^2 k_x^2 + m^2 k_y^2)[(\phi^c_{\ell,m})^2 + (\phi^s_{\ell,m})^2],$$

for $\ell = 1,\cdots,N_x$ and $m=1,\cdots,N_y$.

Anomalous heat transport is characterized by the convective heat flux Γ and Nusselt number Nu, which are defined as

$$\Gamma(x,t) = \int p v_x dy/L_y = \langle p v_x \rangle_y$$

and

$$\text{Nu}(t) = \int (\kappa K_i + p v_x)\frac{dV}{V}/(\kappa K_i) = 1 + \frac{\langle p v_x\rangle_V}{\kappa K_i}.$$

III. DIRECT NUMERICAL SIMULATIONS OF ITG MODEL

In this section, direct numerical solutions of Eqs. (1) and (2) are presented and anomalous transport arising from ITG turbulence is discussed. The parameters used for the simulations are $g=5\times10^{-2}$, $\mu=4\times10^{-3}$, and $\kappa=1\times10^{-3}$. Under these parameters, the instability threshold for parameter K_i is given by $K_{ic}=0.045$. In actual simulations for full PDEs, we employ $N_x=32$ and $N_y=15$, which we have confirmed are large enough to represent the solutions of PDEs, Eqs. (1) and (2), correctly for the parameters used here.

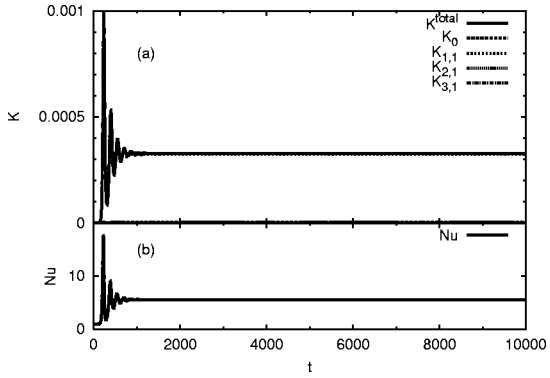

FIG. 1. Time evolutions of (a) kinetic energies K^{total}, K_0, $K_{1,1}$, $K_{2,1}$, and $K_{3,1}$ and (b) the Nusselt number Nu obtained from full PDE simulations for $K_i=0.1$.

When $K_i=0.1$, which is slightly above the threshold, the system reaches a steady state after nonlinear saturation with almost no sheared flow. Figure 1 presents time evolutions of the kinetic energies and Nusselt number under such conditions. In this case, the total kinetic energy K^{total} is essentially equal to that of the $(\ell,m)=(1,1)$ mode and the kinetic energies of other fluctuation components such as K_0, $K_{2,1}$, and $K_{3,1}$ are negligibly small. The trajectory in the phase space for "the kinetic energy of sheared mean flow K_0 vs Nusselt number Nu" and the power spectrum density of kinetic energy $K_{1,1}$ are shown in Figs. 2(a) and 2(b), which indicate that the system converges to a fixed point, i.e., a fixed steady state.

Figure 3 shows time evolutions of the kinetic energies and Nusselt number, Fig. 4(a) the trajectory in the phase space "K_0-Nu," and Fig. 4(b) the power spectrum density of $K_{1,1}$ for $K_i=0.2$. Unlike Fig. 1, the system first reaches and stays in a steady state with higher anomalous transport (i.e., Nu) for a while and then moves to another steady state with lower anomalous transport and a larger sheared mean flow (i.e., K_0). This transition from a high Nu state to a low Nu state with the increase of sheared mean flows may remind one of an *L-H* transition (i.e., transition from a low confinement mode to a high confinement mode) observed in tokamaks. Similar *L-H*-like transitions are also seen in the solutions of the low-degree-of-freedom models.[10]

Figure 5 shows that, with the increase of K_i up to $K_i=0.3$, the system bifurcates to a periodic oscillatory state. The trajectory in the phase space K_0-Nu is attracted to a limit cycle, as shown in Fig. 6(a). The power spectrum density shown in Fig. 6 also indicates such periodicities.

When K_i is further increased, chaotic oscillations appear. Figure 7 shows time evolutions of the kinetic energies and Nusselt number for $K_i=0.9$. Figures 8(a) and 8(b) give the trajectory in the phase space K_0-Nu and the power spectrum density for $K_i=0.9$. The trajectory follows a complex path and the power spectrum exhibits continuous components.

In strongly turbulent regime of $K_i \gtrsim 3$, intermittent bursts

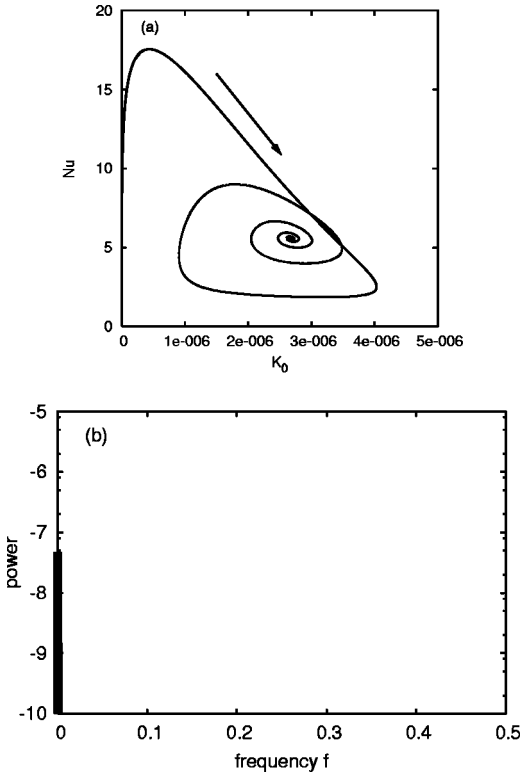

FIG. 2. (a) Trajectory in the phase space "Nu-K_0" and (b) power spectrum density of $K_{1,1}$ obtained from full PDE simulations for $K_i=0.1$.

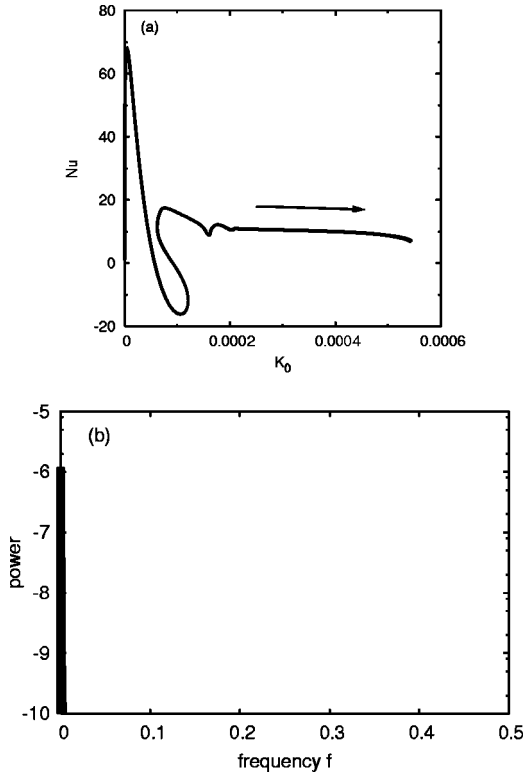

FIG. 4. (a) Trajectory in the phase space Nu-K_0 and (b) power spectrum density of $K_{1,1}$ obtained from full PDE simulations for $K_i=0.2$.

are observed. Figures 9 and 10 show time evolutions of the kinetic energy and Nusselt number for $K_i=5$. Similar to the case discussed in Ref. 10 for the low-degree-of-freedom model, intermittent bursts are caused by nonlinear interactions between the ITG modes and sheared flows also in the case of the full PDE model. As the ITG modes grow, sheared flows are generated by nonlinear coupling of ITG modes. The generated sheared flows then quickly suppress the ITG fluctuations, as indicated by the timing of bursts in $K_{1,1}$ (i.e., ITG fluctuation kinetic energy) and K_0 (i.e., mean flow energy) shown in Fig. 9. After the ITG modes are suppressed, the sheared flows gradually decay due to viscous damping. The time evolution of Nusselt number shown in Fig. 10 also indicates that intermittent bursts of thermal transport synchronize with the growth of fluctuations represented by $K_{1,1}$ in Fig. 9. The power spectrum density of kinetic energy $K_{1,1}$ is given in Fig. 11, which shows larger low frequency components at around $f\sim 0.03$ and 0.08.

We have also evaluated time averaged Nusselt number as in Ref. 10. Dependence of the time averaged Nusselt number Nu on the normalized ion pressure gradient K_i is given in Fig. 12. It is readily seen that there are three transport regimes depending on K_i.

(1) $\mathrm{Nu}\propto K_i^2$ for $K_i \lesssim 0.1$, where the system converges to a fixed steady state.

(2) $\mathrm{Nu}\propto K_i^{1/2}$ for $0.4\lesssim K_i \lesssim 3$, where the system is in the bifurcation stages from periodic to chaotic oscillations.

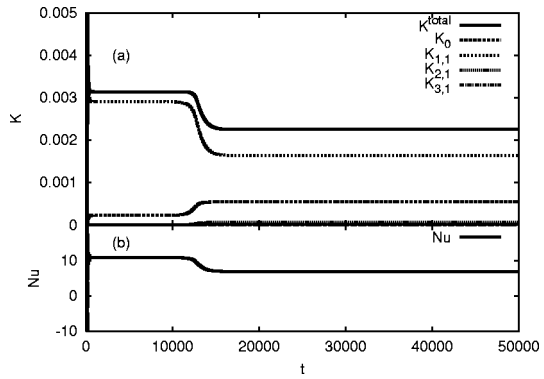

FIG. 3. Time evolutions of (a) kinetic energies K^{total}, K_0, $K_{1,1}$, $K_{2,1}$, and $K_{3,1}$ and (b) the Nusselt number Nu obtained from full PDE simulations for $K_i=0.2$.

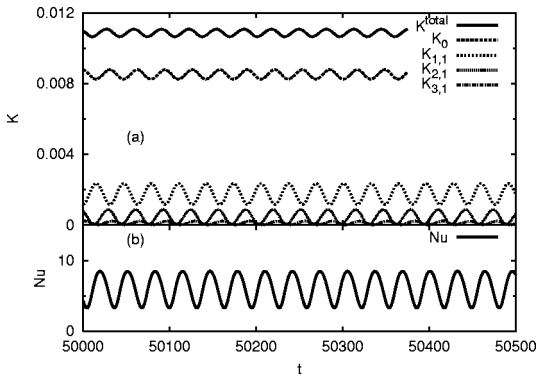

FIG. 5. Time evolution of (a) kinetic energy for K_0, $K_{1,1}$, $K_{2,1}$, and $K_{3,1}$ and (b) the Nusselt number Nu as a result of full PDE simulations. Here $K_i=0.3$.

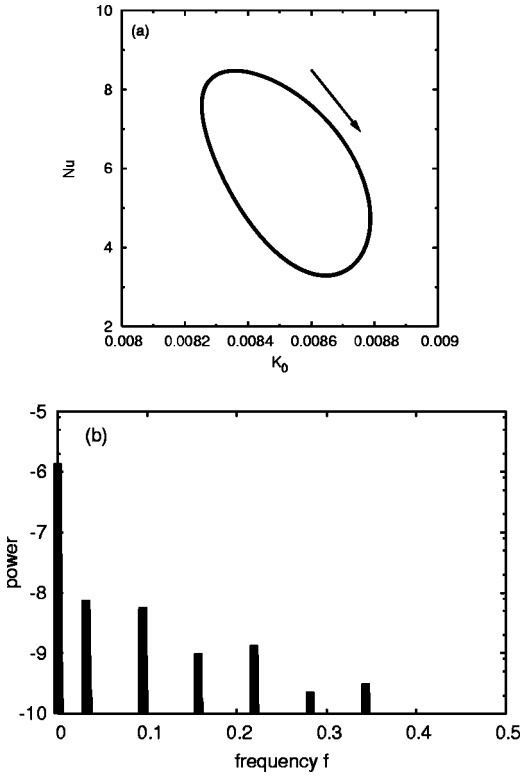

FIG. 6. (a) Trajectory in the phase space Nu-K_0 and (b) power spectrum density of $K_{1,1}$ obtained from full PDE simulations for $K_i=0.3$.

(3) $\mathrm{Nu}\propto K_i^{1/3}$ for $K_i \gtrsim 3$, where intermittent bursting transport occurs.

It is interesting to note that the scaling $\mathrm{Nu}\propto K_i^{1/3}$ in the strongly unstable regime shown here is similar to those observed for Rayleigh–Bénard convections[20,21] and resistive interchange turbulence.[22] We also note that, in the 18 ODE model presented in Ref. 10, the anomalous thermal transport scales as $\mathrm{Nu}\propto K_i^3$ in the strongly unstable regime, which is different from the scaling above. Although the low-degree-of-freedom model seems to capture the essential mechanisms of turbulence intermittency, it fails to reproduce the quantitatively correct anomalous thermal transport.

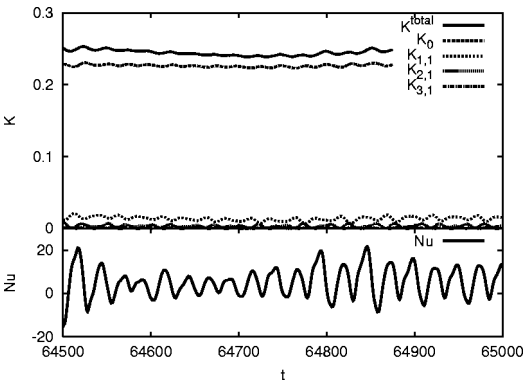

FIG. 7. Time evolution of (a) kinetic energy for K_0, $K_{1,1}$, $K_{2,1}$, and $K_{3,1}$ and (b) the Nusselt number Nu as a result of full PDE simulations. Here $K_i=0.9$.

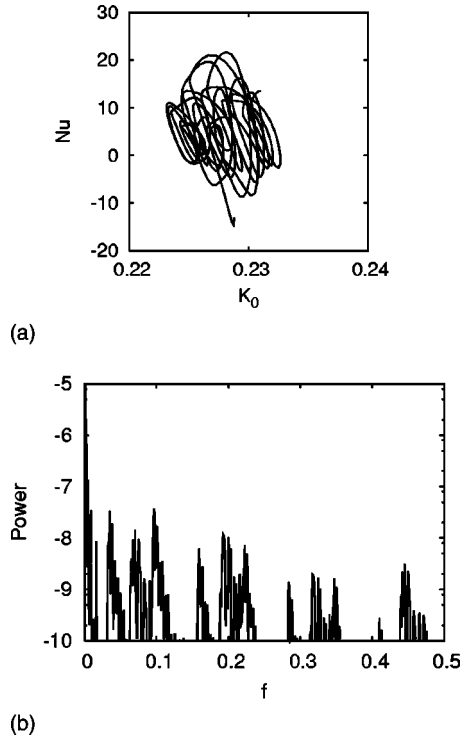

FIG. 8. (a) Trajectory in a phase space Nu-K_0 and (b) power spectrum density of $K_{1,1}$ for the full PDE system. Here $K_i=0.9$.

IV. ONE-DIMENSIONAL SIMULATIONS

As shown in the preceding section, the anomalous thermal transport scalings differ significantly between the full PDE model and the 18 ODE model. The lack of high wave number components in the 18 ODE model must be the reason for this discrepancy. In the real space, this means that the system needs sufficiently fine structures of the modes to correctly represent the amount of heat transport carried by turbulent convection cells. In this section, we therefore examine where the essential structures of the modes need to be kept for a better description of turbulent thermal transport in simplified equations. To this end, we solve a simpler nonlinear system derived from Eqs. (1) and (2), which retains only the

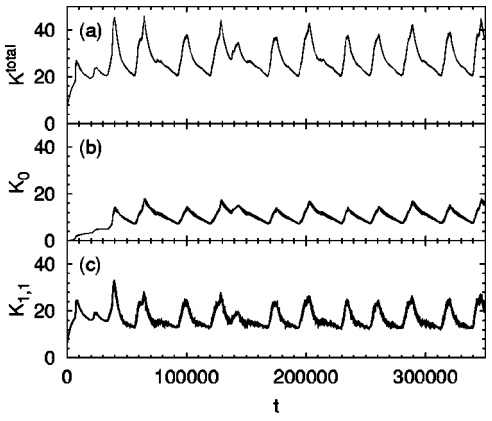

FIG. 9. Time evolution of the total kinetic energy K^{total} and kinetic energy components K_0 and $K_{1,1}$ obtained from full PDE simulations for $K_i=5$. Other Fourier components are negligibly small compared with those listed here.

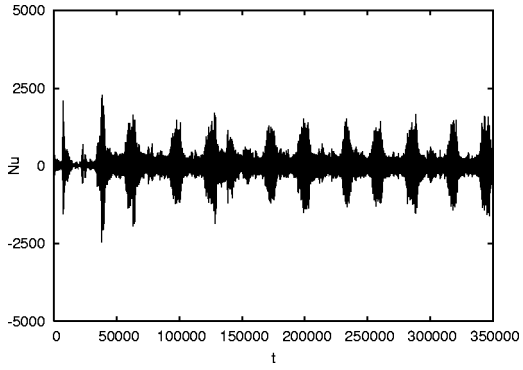

FIG. 10. Time evolution of the Nusselt number Nu obtained from full PDE simulations for $K_i=5$.

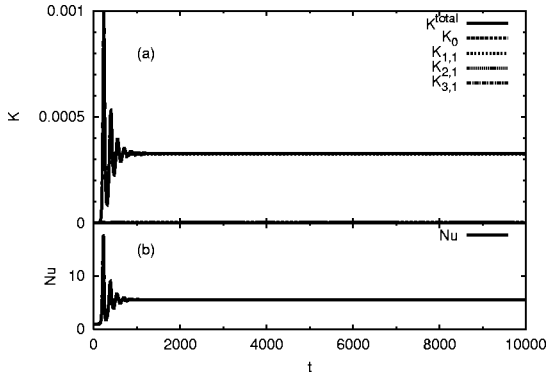

FIG. 13. Time evolutions of (a) kinetic energies K^{total}, K_0, $K_{1,1}$, $K_{2,1}$, and $K_{3,1}$ and (b) the Nusselt number Nu obtained from 1D simulations for $K_i=0.1$.

fundamental and $m=0$ modes in the poloidal direction and a large number of harmonics in the radial direction. We call this system 1D model and, in actual simulations, we set $N_x=64$ and $N_y=1$ for Eqs. (4) and (5).

As in the case of the full PDE model, when the normalized ion pressure gradient K_i is slightly larger than the instability threshold $K_{ic}=0.045$, initial perturbations given to the 1D system grow and nonlinearly saturate with almost no sheared flow. Figure 13 shows time evolutions of the kinetic energies and Nusselt number for $K_i=0.1$. As in Fig. 1, the total kinetic energy K^{total} is essentially equal to that of the $(\ell,m)=(1,1)$ mode and the kinetic energies of other fluctuation components such as K_0, $K_{2,1}$, and $K_{3,1}$ are negligibly small. The trajectory in the phase space K_0-Nu and the power spectrum density in this case are shown in Figs. 14(a) and 14(b), which show that the system converges to a fixed steady state. Indeed Figs. 13 and 14 are almost identical to and visually indistinguishable from Figs. 1 and 2 for the full PDE model.

The similarity in the nonlinear evolution of the kinetic energy components and Nusselt number between the full PDE model and 1D model persists for even larger K_i values. We have confirmed that the nonlinear evolution of these quantities for the 1D model for $K_i=0.2$, 0.3, and 0.9 are given by figures visually indistinguishable from Figs. 3–8.

As in the case of the full PDE model, when $K_i \gtrsim 3$, intermittent bursts appear for the 1D model. For larger K_i val-

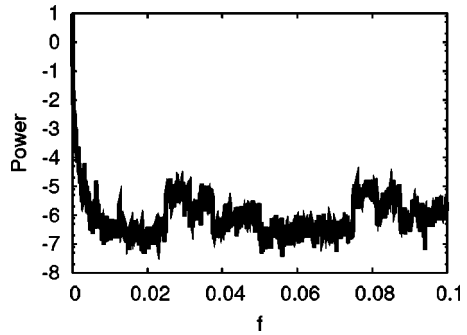

FIG. 11. Power spectrum density of $K_{1,1}$ obtained from full PDE simulations for $K_i=5$.

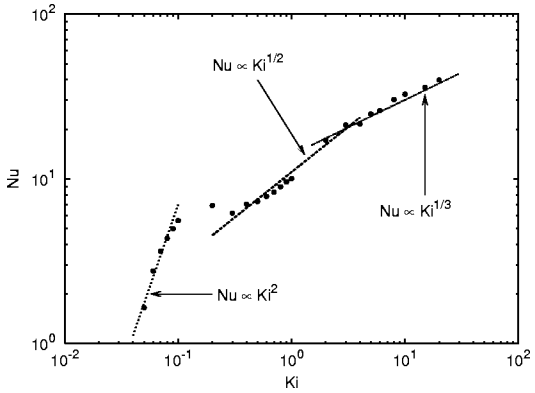

FIG. 12. Time averaged Nusselt number Nu as a function of K_i obtained from full PDE simulations.

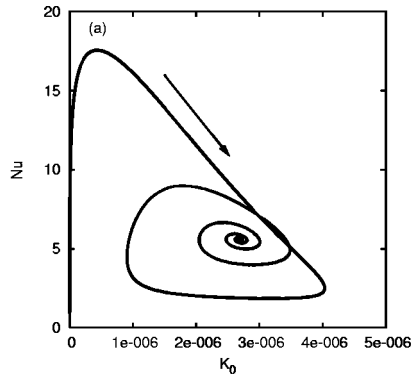

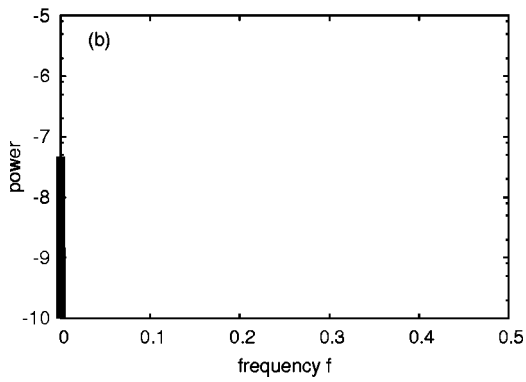

FIG. 14. (a) Trajectory in the phase space Nu-K_0 and (b) power spectrum density of $K_{1,1}$ obtained from 1D simulations for $K_i=0.1$.

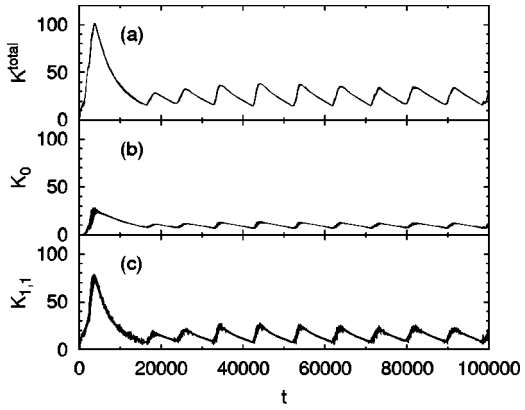

FIG. 15. Time evolution of the total kinetic energy K^{total} and kinetic energy components K_0 and $K_{1,1}$ obtained from 1D simulations for $K_i=5$. Other Fourier components are negligibly small compared with those listed here.

ues, however, one notices some quantitative differences in the nonlinear solutions of the full PDE model and 1D model. Figure 15 shows time evolutions of the kinetic energy components for $K_i=5$, which exhibits intermittent bursts similar, but not identical, to those in Fig. 9. The time evolution of Nusselt number Nu is illustrated in Fig. 16, which shows intermittent bursts that synchronize with the growth of fluctuations $K_{1,1}$, as in Figs. 9 and 10. Note that the amplitudes of Nu bursts are generally larger in the case of the 1D model and also that the time scales of Figs. 10 and 16 are different. The power spectrum density of kinetic energy $K_{1,1}$ is shown in Fig. 17. The spectrum has large components at around $f \sim 0.14$ and 0.42, which indicates that the frequencies of intermittent bursts are also different between the full PDE model and 1D model.

Figure 18 gives the time averaged Nusselt number as a function of K_i. The scaling of the time averaged Nusselt number obtained from the 1D model is surprisingly similar to that from the full PDE model, given the fact that a large number of the higher harmonics in the poloidal direction are ignored in the 1D model. On the other hand, the 18 ODE low-degree-of-freedom model, which has the same mode numbers in the poloidal (i.e., y) directions and only three mode components in the radial (i.e., x) directions, shows a different scaling for the Nusselt number.[10] These facts indicate that the bifurcation dynamics associated with chaotic

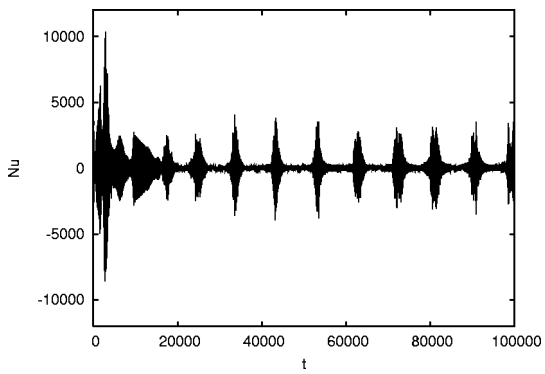

FIG. 16. Time evolution of the Nusselt number Nu obtained from 1D simulations for $K_i=5$.

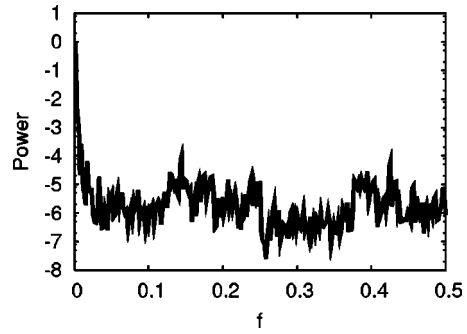

FIG. 17. Power spectrum density of $K_{1,1}$ obtained from 1D simulations for $K_i=5$.

and intermittent oscillations for nonlinear ITG modes strongly depends on the mode structures in the x directions.

V. DISCUSSION

In this work, we have studied anomalous thermal transport due to toroidal ITG driven turbulence using numerical simulation of two different fluid models for toroidal ITG modes, i.e., the full PDE model given by Eqs. (1) and (2) and the 1D model reduced from these equations. In both models, when the normalized ion pressure gradient K_i is slightly larger than the threshold value of instability, the kinetic energy and Nusselt number converge to steady-state values with no sheared mean flow. As K_i is increased, finite sheared flows are generated by nonlinear mode coupling and trigger an L-H-like transition, after which the Nusselt number decreases with the further increase of the sheared mean flow. If K_i is further increased, periodic and chaotic oscillations are observed. When K_i becomes sufficiently large and turbulence becomes strong, intermittent bursts of fluctuating quantities appear.

In both full PDE and 1D models, the Nusselt number Nu scales in a very similar manner with the normalized ion pressure gradient K_i, as shown in Figs. 12 and 18. The scaling may be summarized as follows: (1) $\text{Nu} \propto K_i^2$ when the system converges to a fixed steady state, (2) $\text{Nu} \propto K_i^{1/2}$ when the system is in bifurcation processes from periodic to chaotic oscillations, and (3) $\text{Nu} \propto K_i^{1/3}$ when the system exhibits intermittent bursting transport.

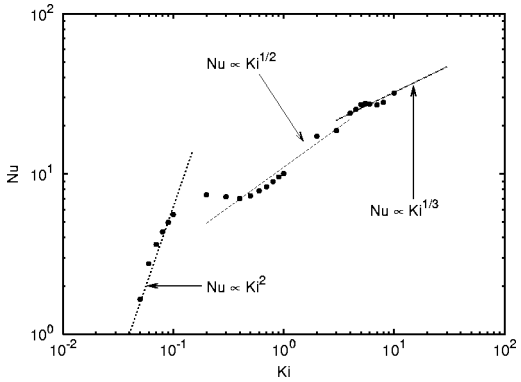

FIG. 18. Time averaged Nusselt number Nu as a function of K_i obtained from 1D simulations.

The similarity in the Nusselt number scaling between the full PDE and 1D models is remarkable, given the fact that only the time-dependent mean component and the lowest order components are retained in the 1D model whereas all poloidal modes are included in the full PDE model. On the other hand, the Nusselt number scaling obtained from the 18 ODE low-degree-of-freedom model[10] is quantitatively different from those obtained from the full PDE and 1D models.

As in the case of the 18 ODE model, we have observed in both full PDE and 1D models that changes of anomalous transport characteristics are caused by the interplay of sheared mean flows and fluctuations. In the first stage where $\mathrm{Nu} \propto K_i^2$, essentially no sheared mean flow is observed. In the next stage, where $\mathrm{Nu} \propto K_i^{1/2}$, the generation of sheared mean flows reduces the growth of ITG instabilities and the reduction of the instabilities reduces the generation of sheared mean flows, which leads to periodic or chaotic oscillations of fluctuating quantities. In the stage where $\mathrm{Nu} \propto K_i^{1/3}$, intermittent bursts of fluctuating quantities occur, which is again caused by similar interactions between sheared mean flows and fluctuations, as discussed in Ref. 10. We also note that the scaling $\mathrm{Nu} \propto K_i^{1/3}$ is similar to those observed for Rayleigh–Bénard convections[20,21] and resistive interchange turbulence.[22] This scaling behavior provides insights into the nature of tokamak plasma turbulence which shares many common features with thermal convective turbulence.

In summary, the 18 ODE low-degree-of-freedom model for ITG modes discussed in our previous work,[10] which contains only the most unstable mode and several low-order harmonics, can qualitatively accounts for the essential dynamics of nonlinear ITG driven turbulence although it fails to reproduce quantitatively correct anomalous thermal transport, which we have obtained by solving the full PDE model in the present work. On the other hand, we have found that the 1D model reduced from the full PDE model can reproduce the anomalous thermal transport scaling similar to that obtained from the full PDE model. These facts indicate that the generation of sheared mean flows due to the nonlinear evolution of toroidal ITG modes and suppression of the instabilities by such flows are largely determined by the dynamics and mode interactions in the radial direction.

ACKNOWLEDGMENTS

This work was supported by Kyoto University 21COE program "Establishment of COE on sustainable energy systems." One of the authors S.B. acknowledges support and hospitality from the Graduate School of Energy Science of Kyoto University and 21 COE program.

[1] B. Coppi, M. N. Rosenbluth, and R. Z. Sageev, Phys. Fluids **10**, 1762 (1967).
[2] W. Horton, R. D. Estes, and C. Biskamp, Plasma Phys. **22**, 663 (1980).
[3] S. Hamaguchi and W. Horton, Phys. Fluids B **2**, 1834 (1990).
[4] S. Hamaguchi and W. Horton, Phys. Fluids B **2**, 3040 (1990).
[5] S. Hamaguchi and W. Horton, Phys. Fluids B **4**, 319 (1992).
[6] W. Horton, D.-I. Choi, and W. Tang, Phys. Fluids **24**, 1077 (1981).
[7] A. Jarmen, P. Anderson, and J. Weiland, Nucl. Fusion **27**, 941 (1987).
[8] H. Nordman and J. Weiland, Nucl. Fusion **29**, 251 (1989).
[9] G. Hu and W. Horton, Phys. Plasmas **4**, 3262 (1997).
[10] K. Takeda, S. Benkadda, S. Hamaguchi, and M. Wakatani, Phys. Plasmas **11**, 3561 (2004).
[11] K. Takeda, S. Hamaguchi, and M. Wakatani, Plasma Phys. Controlled Fusion **44**, A487 (2002).
[12] S. Benkadda, P. Beyer, N. Bian, C. Figarella, O. Garcia, X. Garbet, P. Ghendrih, Y. Sarazin, and P. H. Diamond, Nucl. Fusion **41**, 997 (2001).
[13] P. Beyer, S. Benkadda, X. Garbet, and P. H. Diamond, Phys. Rev. Lett. **85**, 4892 (2000).
[14] Z. Lin, T. S. Hahm, W. W. Lee, W. M. Tang, and P. H. Diamond, Phys. Rev. Lett. **83**, 3645 (1999).
[15] L. Chen, Z. Lin, and R. White, Phys. Plasmas **7**, 3129 (2000).
[16] V. S. Marchenko, Phys. Rev. Lett. **89**, 185002 (2002).
[17] V. S. Marchenko, V. Ya. Goloborod'ko, and S. N. Reznik, Phys. Plasmas **10**, 4913 (2003).
[18] N. Bian, S. Benkadda, O. E. Garcia, J.-V. Paulsen, and X. Garbet, Phys. Plasmas **10**, 1382 (2003).
[19] S. Hamaguchi, Phys. Fluids B **1**, 1416 (1989).
[20] J. R. Herring, J. Atmos. Sci. **23**, 672 (1966).
[21] L. P. Kadanoff, Phys. Today **54**, 34 (2001).
[22] H. Sugama and M. Wakatani, J. Phys. Soc. Jpn. **59**, 3937 (1990).